Title
Practical design of multi-channel MOSFET RF transmission system for 7 T animal MR imaging

Journal
Concepts in Magnetic Resonance Part B, 45(4)

ISSN
1552-5031

Authors
Zhang, Yizhe
Liu, Yan
Sun, Bingyao
et al.

Publication Date
2015-10-01

DOI
10.1002/cmr.b.21313

Peer reviewed

Practical Design of Multi-Channel MOSFET RF Transmission System for 7 T Animal MR Imaging

YIZHE ZHANG,[1] YAN LIU,[1] BINGYAO SUN,[1] XIAOLIANG ZHANG,[2,3] XIAOHUA JIANG[1]

[1] *Department of Electrical Engineering, Tsinghua University, Beijing, China*
[2] *Department of Radiology and Biomedical Imaging, University of California San Francisco (UCSF), San Francisco, CA*
[3] *UCSF/UC Berkeley Joint Bioengineering Program, San Francisco, CA*

ABSTRACT: In this work, we developed and tested a multi-channel radio frequency (RF) transmission system with compact metal-oxide semiconductor field effect transistor (MOSFET) amplifiers for parallel excitation in 7 T animal MRI scanner. The system is composed of a multi-channel RF controller and four independent RF power amplifiers. Each power amplifier contains two amplification stages. The design was validated by simulation and bench test. The power gain for the amplifier is 18.7 dB at 300 MHz, demonstrating the sufficient amplification capability of the transmission system for small animal parallel excitation applications at 7 T. This compact RF power amplifier can be potentially used for on-coil amplification in multichannel RF array system. Concepts Magn Reson Part B (Magn Reson Engineering) 45B: 191–200, 2015

KEY WORDS: parallel excitation; MOSFET; multi-channel transmission system; radio frequency (RF); power amplifiers

I. INTRODUCTION

Parallel excitation using multi-channel transmission systems (*1–4*) is capable of addressing the problems of radio frequency (RF) field inhomogeneity and increased local specific absorption rate (SAR) at ultrahigh magnetic fields (7 Tesla and above) (*5–9*). Since the phase and amplitude of each transmit channel can be independently controlled, multi-channel transmit array can be used for $B1$ shimming and obtaining more uniform $B1$ distribution than single channel. The parallel excitation method enables an optimized RF excitation profile, which can optimize SAR and make ultrahigh field MRI safer (*8,10,11*). Moreover, multi-channel transmission can provide a fast and efficient approach to performing selective excitation (*1,2*). Because of these unique advantages, multichannel parallel excitation technique is advocated for high and ultrahigh field MR imaging applications despite the technical challenges of designing the required high frequency RF transceive arrays (*12–21*).

However, currently multi-channel transmission systems are not equipped in most MR scanners, and researchers have been prototyping multi-channel transmitters that are cost-effective and easy to be integrated to the existing MR scanners, and are with high power and efficiency. Another important requirement for RF transmitters is their high accuracy, or linearity (*22–24*). Non-linearities may lead to errors in the slice definition, and may lead to more severe problems depending on the employed sequence (*24*). In the work by Hollingsworth et al. (*24*), an eight channel transmit system for parallel excitation at 3 T was developed that can provide a high level of decoupling between coil elements.

Received 22 June 2015; revised 2 October 2015; accepted 4 October 2015

Correspondence to: Xiaohua Jiang; E-mail: jiangxiaohua@mail.tsinghua.edu.cn or Xiaoliang Zhang; E-mail: xiaoliang.zhang@ucsf.edu

Concepts in Magnetic Resonance Part B, Vol. 45B(4) 191–200 (2015)

Published online in Wiley Online Library (wileyonlinelibrary.com). DOI: 10.1002/cmr.b.21313

Linearity is guaranteed by using a predistortion correction method. In Ref. 25, Gudino et al. proposed an on-coil multiple channel transmit based on class-D operation. Given its compact size and reasonably high RF power output capability, on-coil metal-oxide semiconductor field effect transistor (MOSFET) RF amplifier offers advantages for practical implementation of parallel excitation (*25,26*). Additionally this active device, MOSFET, holds the promise of delivering RF power while functioning in the high magnetic field environments (*27*). In this work, we develop a multi-channel transmission system with compact MOSFET amplifiers for 7 T animal MRI scanner. Comparing with the large-sized human imaging applications, animal MR studies usually involve much reduced imaging volume, thus less RF power required for spin excitation, which makes MOSFET amplification more suitable and practical for animal MR signal transmission. This compact RF power amplifier can be potentially used for on-coil amplification in the multichannel RF systems. The related circuit design is described and analyzed in detail and its performance is evaluated experimentally through standard RF testing procedures.

CONSIDERATIONS IN RF POWER AMPLIFIER DESIGN

The stability of the amplifier, impedance matching, and electro-magnetic interference (EMI) are the key considerations in the design of an RF power amplifier.

Stability

In an RF transmission network, if the reflection coefficient of a certain port, $|\Gamma_0|$, is greater than 1, positive feedback will be introduced which may cause the amplifier unstable (*28*). In order to ensure unconditional stability, the real part of the impedance of the signal source, the load, the amplifier input, and the amplifier output, respectively, should be greater than 0. The derived necessary and sufficient conditions for unconditional stability are $K>1$ and $A>0$, where K is the stability factor and $K=\frac{1-|S_{11}|^2-|S_{22}|^2+|\Delta|^2}{2|S_{12}S_{21}|}$, A is the auxiliary stability factor and $A=1+|S_{11}|^2-|S_{22}|^2-|\Delta|^2$, and $\Delta=S_{11}S_{22}-S_{12}S_{21}$ (*29*).

Impedance Matching

To maximize the power gain and output power of the power amplifier, impedance matching networks at the input and output ports of the amplifier need to be designed for ensuring minimal power reflection. The impedance matching network can be realized by lumped element circuits or distributed parameter circuits. Lumped element circuits are simple for analyzing and are suitable for impedance matching at the low end of GHz frequencies or lower. The amplifier designed in this work adopts lumped element circuits for impedance matching and the matching circuits are designed using Smith charts.

Electro-Magnetic Interference

EMI is disturbance that affects a device or system due to electro-magnetic emissions from an external source (*30*). Owing to the high operating frequency and high power level of the RF power amplifier in the MR imaging applications at ultrahigh fields, EMI may significantly degrade the performance of the amplifier circuit. Thus in schematic design and printed circuit board (PCB) layout design, measures need to be taken to reduce the negative effects of EMI.

METHODS

The multi-channel transmission system used in MR system is composed of a multi-channel RF controller and independent RF power amplifiers. The PC graphic user interface (GUI), microcontroller, and digital analog converter (DAC) constitute the RF controller. The phase shifter, attenuator, and the two-stage amplification constitute the RF power amplifier.

Multi-Channel RF Controller

The PC GUI (developed based on LabVIEW, National Instruments, Santa Clara, CA) is used for setting the phase and amplitude of each channel of transmission. The serial port signal from PC is processed by the microcontroller (STC11F04E, STCmicro Company, Beijing, China). The output digital signal from the microcontroller is converted into analog voltage of 0–10 V by the 12-bit DAC (DAC7678, Texas Instruments, Dallas, Tx). DAC7678 has eight output channels which are used to control the voltage-controlled phase shifters and attenuators (*4*).

RF Power Amplifier

The designed center operating frequency of the RF power amplifiers for 7 T MR applications are 300 MHz. Each channel of RF power amplifier contains one phase shifter, one attenuator, and two stages of power amplification. The RF signal is shifted in

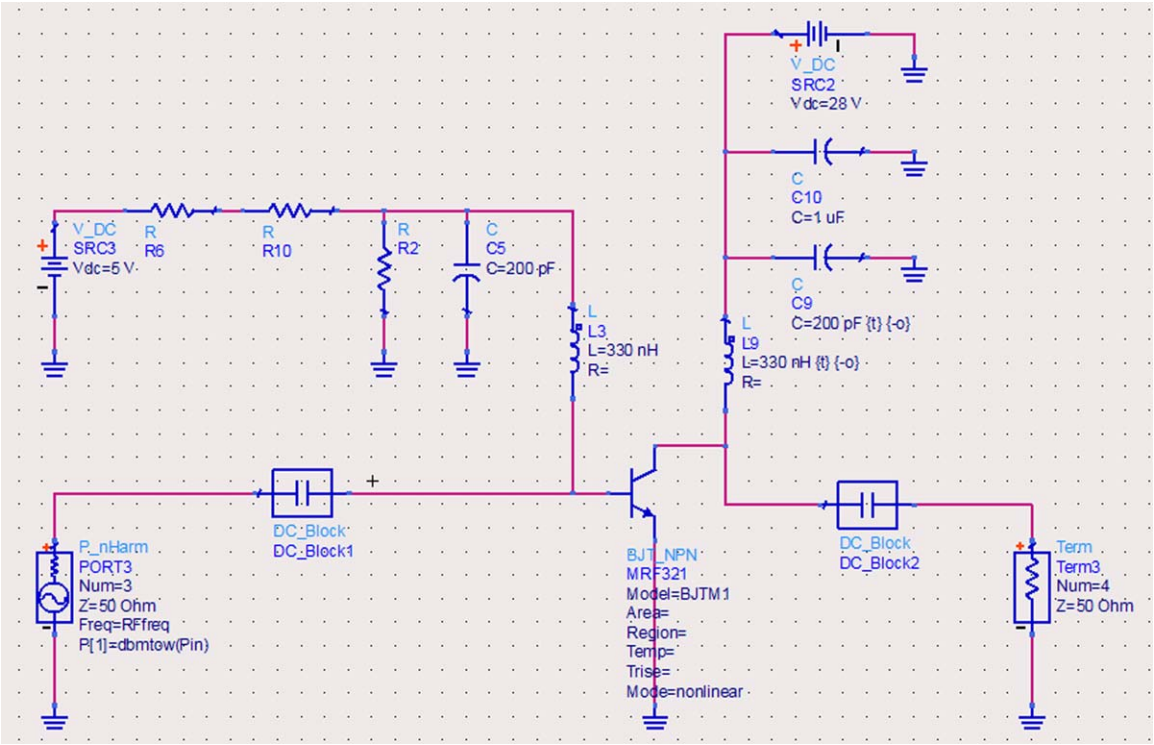

Figure 1 DC bias circuit for the first stage amplification.

phase and attenuated in amplitude to obtain the designed waveform, and then amplified by the two-stage power amplification. The voltage-controlled phase shifter (JSPHS-42+, Mini-Circuits, Brooklyn, NY) and attenuator (MVA-2000+, Mini-Circuits, Brooklyn, NY) have phase shift ranging from 0° to 200° and attenuation ranging from 2 dB to 43 dB with control voltage of 0–10 V. In the two-stage power amplification, the first stage uses power transistor (MRF321, 10W rated, M/A-COM, Lowell, MA) and the second stage uses power MOSFET (MRF177, 100W rated, M/A-COM, Lowell, MA). In the amplifier design, Class A operation was employed for gaining high linearity. We used ADS (Advanced Design System, Agilent Technologies, Santa Clara, CA) and Altium Designer (Altium Company, La Jolla, CA) for the schematic design and the PCB design respectively.

Schematic Design. The schematic design of the amplifier addresses the issues of setting the DC operating points, ensuring circuit stability and impedance matching.

DC bias circuit. The V_{CE} of MRF321 is set to be 28 V as recommended in the datasheet, and the designed DC bias circuit for the first stage amplification is shown in Fig. 1.

In the circuit shown in Fig. 1, the components R_6, R_{10}, and R_2 are for setting the base current of the transistor to the proper value, C_5 and L_3 as well as C_9 and L_9 prevent the RF currents from getting to the DC sources, C_{10} filters the noise of the DC source.

The V_{DS} of MRF177 is set to be 28 V as recommended in the datasheet, and the designed DC bias circuit for the second stage amplification is shown in Fig. 2.

The components R_{23} and R_{24} are for setting the gate voltage of the MOSFET to the proper value, R_7 limits the current, C_{28} and L_5 as well as C_{12} and L_6 prevent the RF currents from getting to the DC sources, C_{25} and C_{27} filter the noise of the DC sources.

Ensuring circuit stability. If an amplifier is potentially unstable in the operation band, measures should be taken to ensure its unconditional stability. As stated in section "Stability," the real part of the amplifier input impedance and output impedance should be greater than 0 to achieve unconditional stability. When any of both is smaller than 0, a common measure to ensure stability is to add a

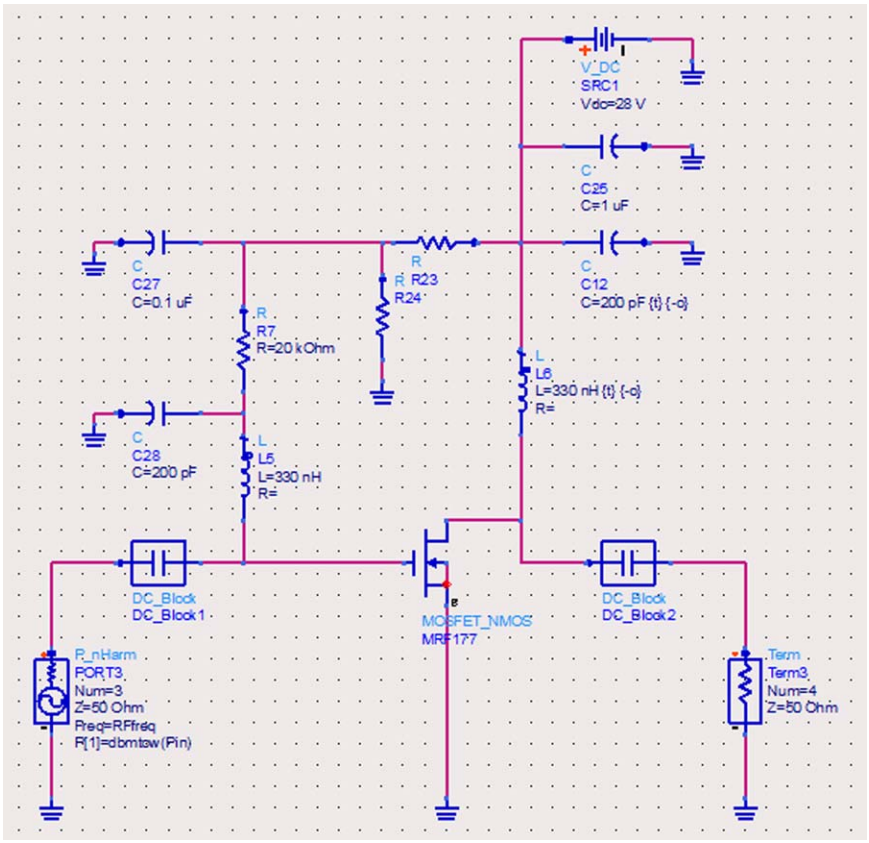

Figure 2 DC bias circuit for the second stage amplification.

resistor at the input or output port to counteract the negative real part. The resistor for ensuring circuit stability is added at the input port rather than the output port (Fig. 3) in consideration of minimizing the power consumption of the resistor. Although a resistor at the input and output port may both fulfill the function of stabilization, its power consumption at the input port would be much smaller since the power and current are much lower at the input than output port.

While a resistor can help to ensure stability, it will decrease the power gain of the amplifier and cause additional power loss. The greater the series resistance value, the larger the stability margin, but, as a trade-off, the lower the power gain and the efficiency of the amplifier. To determine the proper resistance value, simulation studies are carried out. The stability factors of the amplifier with different resistor values are calculated by simulation. Take the second stage amplifier as an example. Table 1

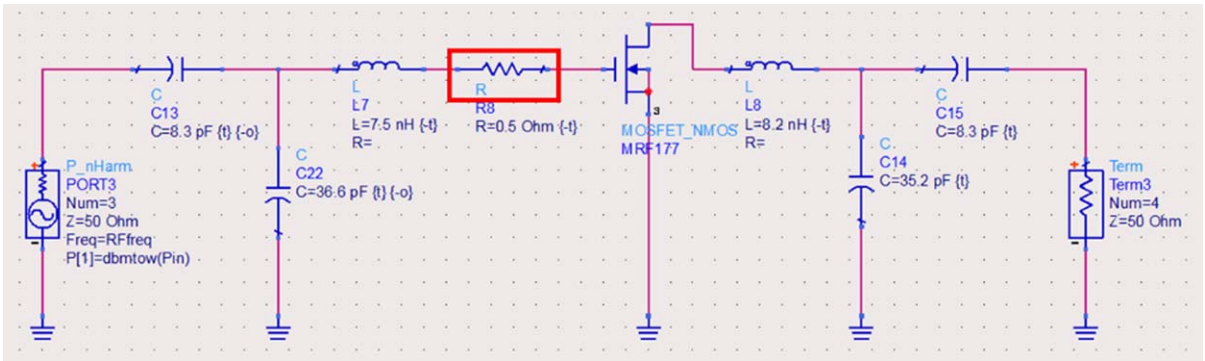

Figure 3 Adding a resistor at the input port to ensure stability.

Table 1 Stability Factors (K and A) of the Amplifier With Different Resistor Values

Resistance (Ω)	*K*	*A*
0	1.01	0.28
0.25	1.24	0.74
0.5	1.46	0.84
0.75	1.68	0.89
1	1.90	0.92

shows the stability factor K and the auxiliary stability factor A of the amplifier at 300 MHz.

As shown in the table, when the resistance is 0 (without the resistor for ensuring stability), $K = 1.01$, $A = 0.28$. These two factors show that the circuit without the resistor is slightly above the threshold for stability ($K > 1$, $A > 0$) at 300 MHz. But variances in component parameters may easily cause K to become less than 1, and the amplifier to be potentially unstable. Also, at frequencies adjacent to 300 MHz, K may become less than 1. These show the necessity of adding a resistor for guaranteeing the stability of the amplifier at around 300 MHz. When the resistance increases from 0 to 1 Ω, K and A both increase to be greater than their threshold values and the stability margin is enlarged. The criteria for determining the proper resistance value are i) the stability margin under this resistance value should be large enough, ii) the resistance should not be too large so as to avoid serious negative impact on power gain and efficiency, and iii) the resistance should be a commonly-used value that is available for purchase. When the resistance is 0.5 Ω, $K = 1.46$ and $A = 0.84$, and the amplifier is unconditionally stable with an appropriate stability margin. Also 0.5 Ω is not a value too large that can cause serious negative effects, and it is a commonly-used resistance value. Therefore, the resistor in the second stage amplifier is chosen to be 0.5 Ω (Fig. 3). Similar measures are used for determining the proper resistance value in the first stage amplifier.

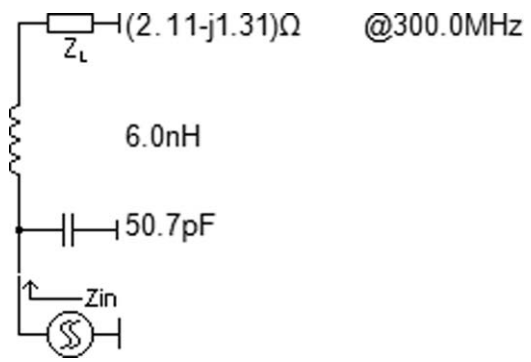

Figure 4 The configuration of the L-section matching network.

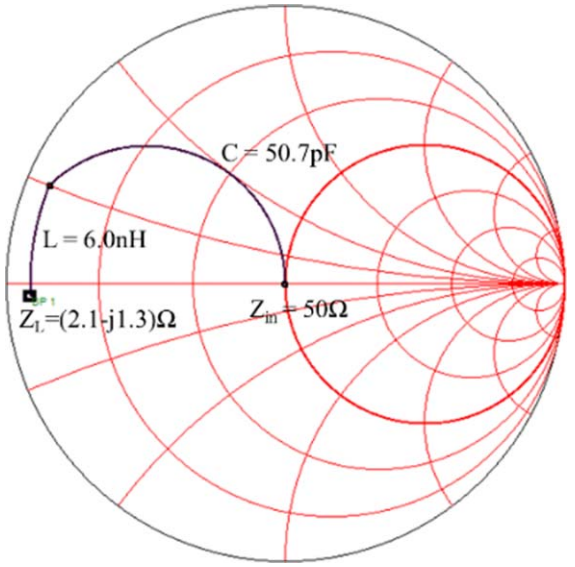

Figure 5 The Smith chart of the L-section matching network.

Impedance matching network. Impedance matching networks using lumped element circuits have three typical types: L-section network, π-section network, and T-section network (*29*).

In this RF amplifier design, theoretically either of those three networks can be used for impedance match. L-section networks have relatively simple topology comprising only two elements. In this specific design, the input impedance of transistor MRF177 (containing the 0.5 Ω resistor for ensuring stability) measures $(2.1 - j1.3)$ Ω at 300 MHz. To match this impedance to, for example, 50 Ω, an impedance matching network can be designed using an L-section network as shown in Fig. 4 for the network topology and Fig. 5 for the corresponding Smith chart. As indicated in this design, the capacitance of the matching capacitor is 50.7 pF while the inductance of the matching inductor is 6.0 nH.

Unlike L-section matching network, π-section or T-section matching network has three components

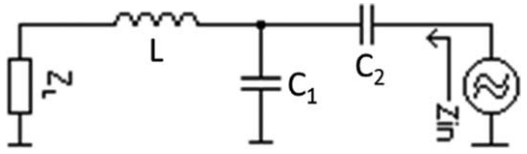

Figure 6 The configuration of the T-section matching network.

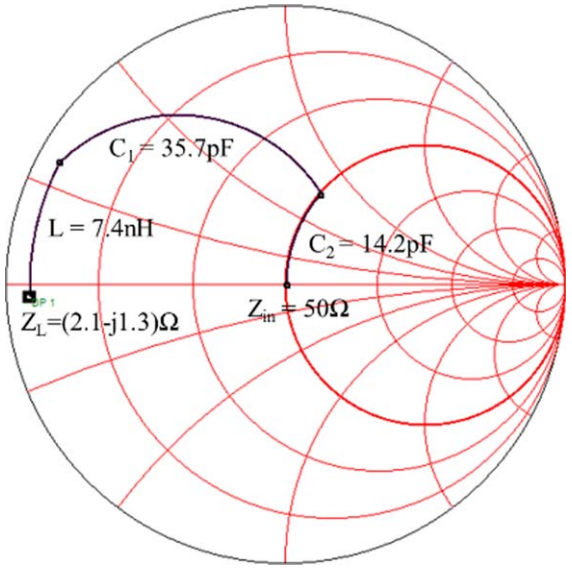

Figure 7 The Smith chart of the first combination of component values.

which may increase complexity of the circuit at certain level but offers more choices in selecting component values and gain more freedom in practical circuit designs. For instance, if a T-section circuit is used to match the impedance of $(2.1 - j1.3)$ Ω to 50 Ω based on the circuit topology as shown in Fig. 6, the inductor and capacitors could have different combinations of values, for example, $L = 7.4$ nH, $C_1 = 35.7$ pF, $C_2 = 14.2$ pF or $L = 12.2$ nH, $C_1 = 19.8$ pF, $C_2 = 5.7$ pF. The corresponding

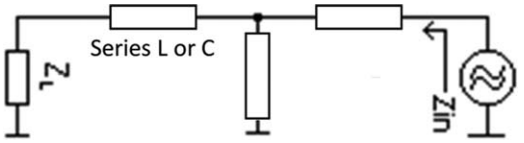

Figure 9 T-section network.

Smith Charts for these two combinations are shown in Figs. 7 and 8, respectively.

In this work, a T-section matching network is employed for impedance matching in the proposed RF amplifiers, and its configuration is shown in Fig. 6. The π-section matching network is not used because it is not as suitable for impedance matching for the amplifier in this work. Take the matching for the input impedance of transistor MRF177 (second stage amplifier) as an example. The impedance is $Z_L = (2.1 - j1.3)$ Ω and it is to be matched to $Z_{in} = 50$ Ω. When employing a T-section network (Fig. 9), the first component is connected to Z_L in series, and it can be a series L or a series C. In the T-section network matching, impedance Z_L can be first transformed to impedance Z_1 by the series L or series C, and then transformed to impedance Z_2 and finally to $Z_{in} = 50$ Ω, as shown by the Smith chart in Fig. 10. While for a π-section network (Fig. 11), the first component is connected to Z_L in parallel, and it can be a parallel L or a parallel C. In the π-section network matching, impedance Z_L can be first transformed to impedance Z_1 by the parallel L or parallel C as shown by the Smith chart in Fig. 12. However, as shown, this transformation cannot alter

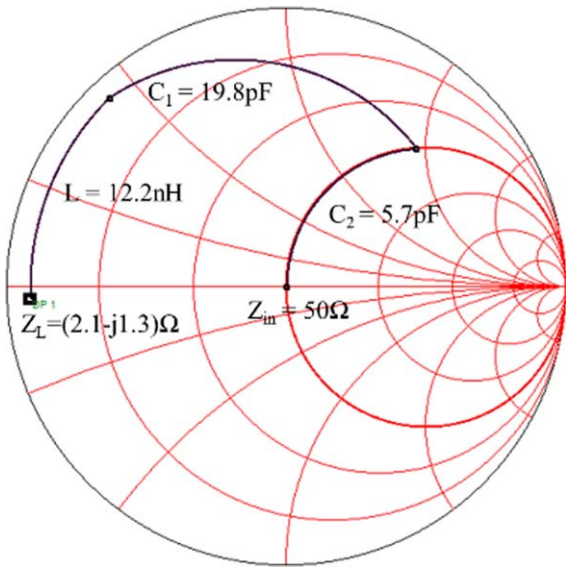

Figure 8 The Smith chart of the second combination of component values.

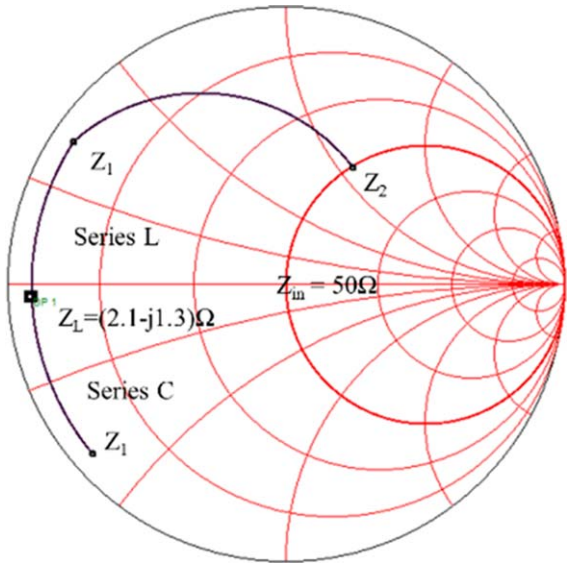

Figure 10 The Smith chart for T-section network matching.

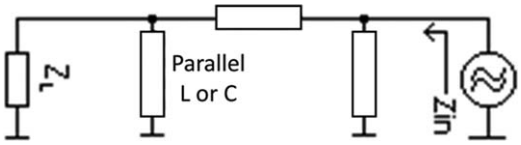

Figure 11 π-section network.

the impedance value largely, and is not very beneficial for finally transforming the impedance to $Z_{in} = 50\ \Omega$, which is at the center of the Smith circle. Therefore, π-section network is not suitable for impedance matching here.

PCB Design. When designing the PCB of the RF circuit, the following strategies are applied to minimize the impact of EMI.

1. Decrease the distance between two connected components. Increase the width of the lines where RF signals flow and where large DC source currents flow. Use two-layer board, and place ground copper on the entire bottom layer and the unused areas of top layer in order to increase the area of the ground.
2. From the left to the right of the board place sequentially the RF input, the first stage amplification, the second stage amplification, and the RF output, so that the RF signals flow directly from left to right. Arrange circuits of different functions in different regions of the board. The upper half of the board is the DC bias circuit region, and the lower part is the impedance matching region where the RF signals flow.

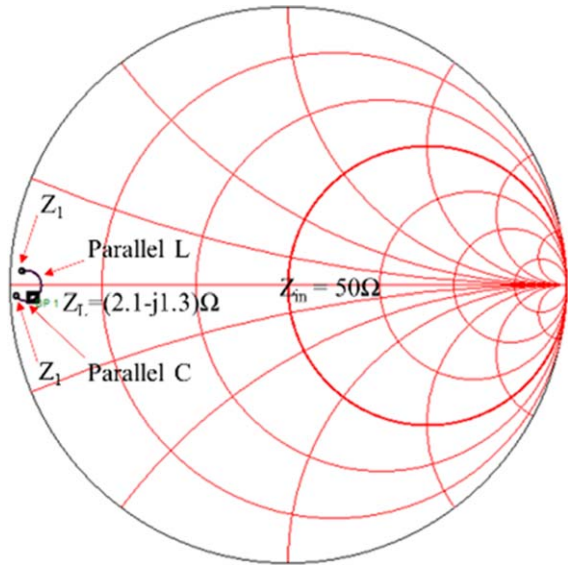

Figure 12 The Smith chart for π-section network matching.

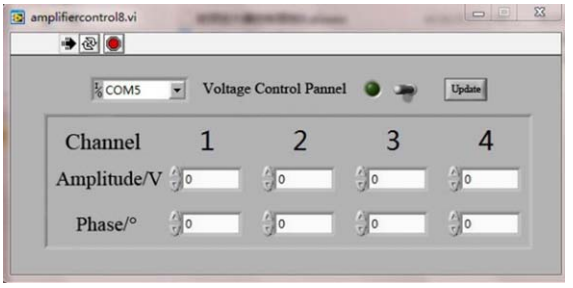

Figure 13 GUI on PC for controlling the amplitude and phase of each transmission channel.

RESULTS

Multi-Channel RF Controller

The PC GUI designed for the 4-channel control is shown in Fig. 13. To test the RF controller, different voltage values are set in the PC GUI and the output voltage values in the DAC are measured (Fig. 14). The output in the DAC is expected to be equal to the input from the PC GUI.

RF Power Amplifier

Figure 15 shows the schematic of the power amplifier design. The amplifier performance is simulated using ADS. Taking the second stage amplifier as an example, the simulation results at 300 MHz are: stability factor $K = 1.46$, auxiliary stability factor $A = 0.84$ (Fig. 16), reflection coefficient $S_{11} = -44.2$ dB, transmission coefficient $S_{21} = 13.8$ dB, voltage standing wave ratio (VSWR) = 1.01 (Fig. 17).

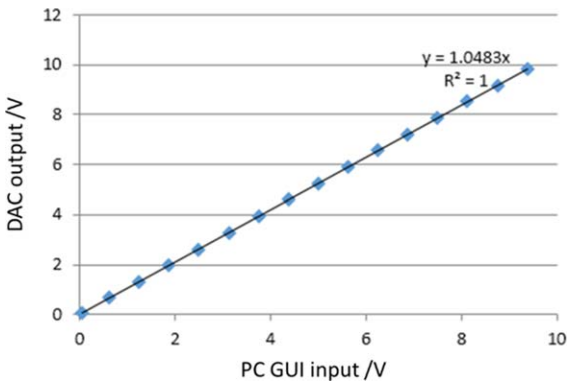

Figure 14 Voltage values set in the PC GUI vs. the output voltage values in the DAC.

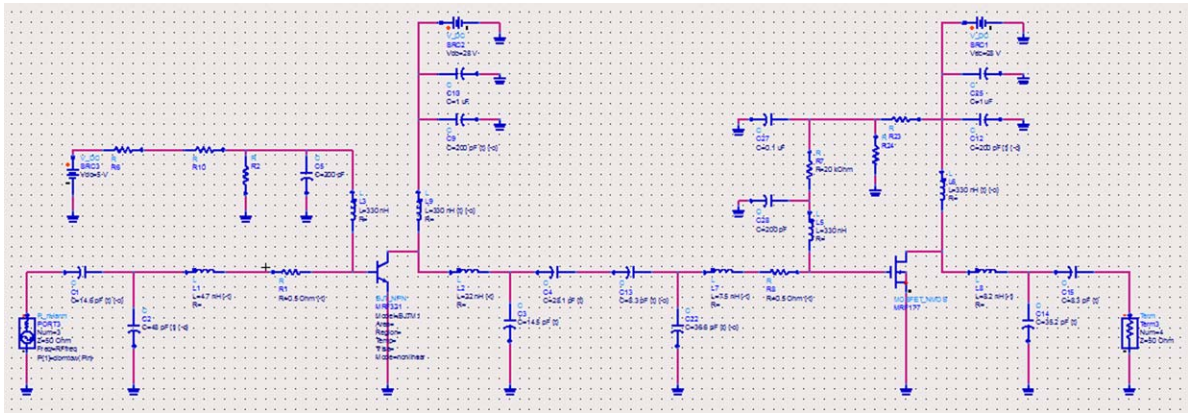

Figure 15 Schematic of the two-stage RF power amplifier using MOSFET.

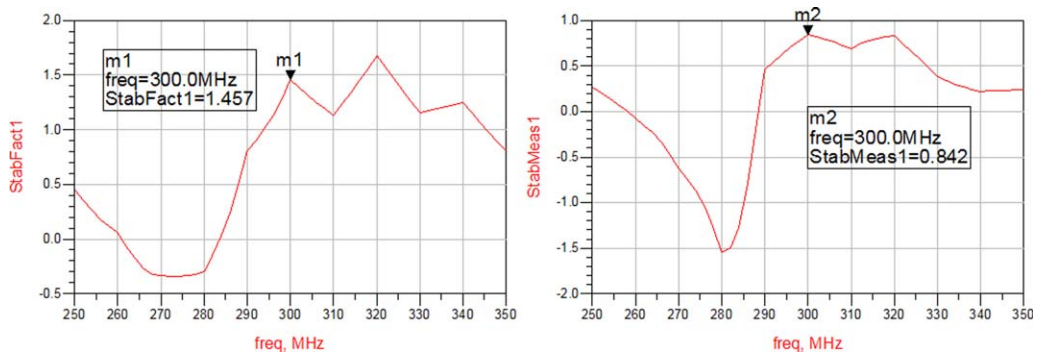

Figure 16 Simulation results: K, A of the second stage MOSFET amplifier.

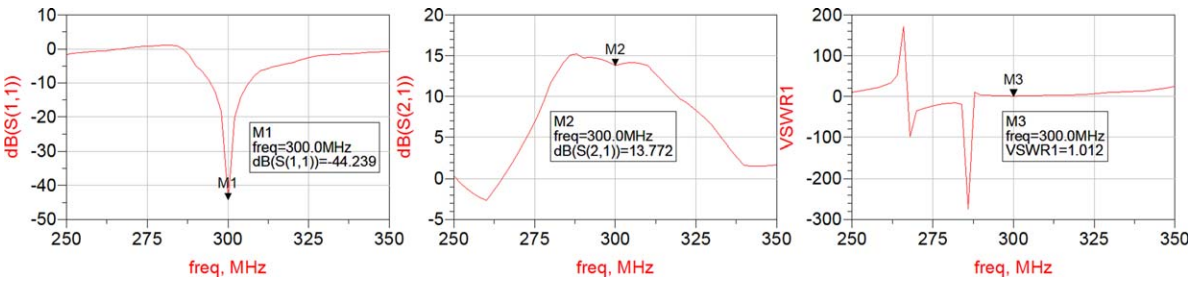

Figure 17 Simulation results: $S11$, $S21$, VSWR of the second stage MOSFET amplifier.

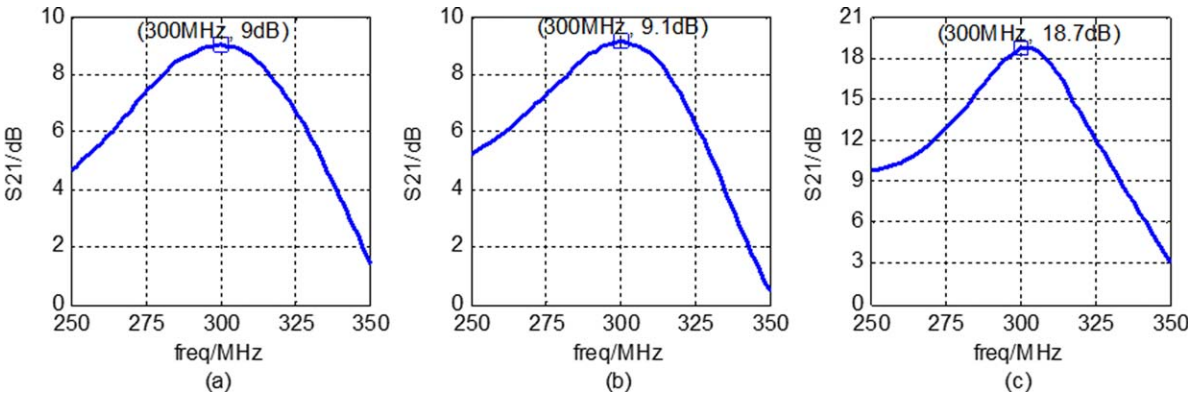

Figure 18 Power gain ($S21$) of (a) the first stage amplifier, (b) the second stage amplifier, and (c) the entire amplifier vs. operation frequency.

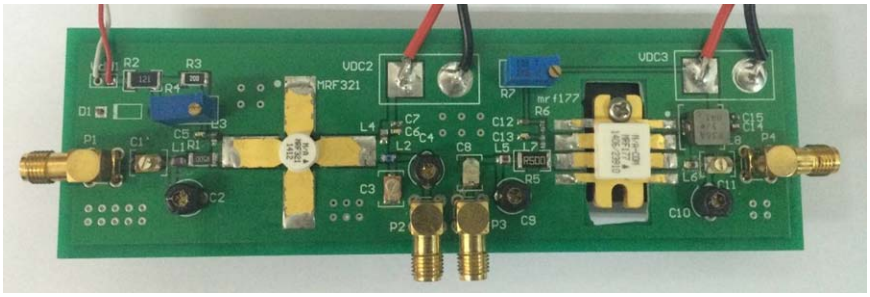

Figure 19 Photograph of one of the MOSFET RF power amplifiers developed for 7 T small animal imaging system

The amplifier is tested with a calibrated network analyzer. The center operating frequency of the amplifier is 300 MHz. At this frequency, the power gain of the first stage amplifier, second stage amplifier, and the entire amplifier is 9.0 dB, 9.1 dB, and 18.7 dB, respectively (Fig. 18). Figure 19 illustrates the prototype amplifier designed for one of the channels in the multichannel transmitter for MR parallel excitation.

DISCUSSION

Multi-Channel RF Controller

Figure 14 shows an excellent linear relationship between the input and the output, with the correlation coefficient equal to 1. The slope of the fitted line is 1.0483. The maximum error is 0.46 V, when the input is 9.5 V and the output is 9.96 V. The possible sources of the error are as follows:

1. When the analog value (the phase shift or the attenuation value set by the PC GUI) is converted into a digital value in PC. Due to the limitation of the bit number of the digital value, error from this source cannot be corrected.
2. When the digital value is converted back to an analog value in DAC. Error from this source can be corrected by processing the data at the input, i.e., by dividing the input phase shift and attenuation values by the slope 1.0438 in the PC GUI.

RF Power Amplifier

In the simulation of the second stage power amplifier, $K = 1.46 > 1$ and $A = 0.84 > 0$, showing that the amplifier is unconditionally stable at 300 MHz. The simulation results $S_{21} = 13.8$ dB, $S_{11} < -20$ dB, VSWR ≈ 1 show that the amplifier has high power gain (S_{21}) and negligible reflected energy loss. In the bench test, the power gains of the first, second stage, and the entire amplifier are at high level, providing sufficient amplification of the transmission system at 300 MHz for small animal parallel excitation applications at 7 T. The bench test results are basically consistent with the simulation results. One possible error source may be the difference between the nominal value and the true value of the electric components used in the amplifier circuits. By fine tuning the parameters of the amplifier circuits, further improvement of amplification gain can be expected.

VI. CONCLUSION

In this work, the design of a multi-channel transmission system with compact MOSFET amplifiers for 7 T small animal MR imaging system is presented. Bench test of the multi-channel RF controller shows the high accuracy of the controller. The amplifier design was validated by simulation and bench test through standard RF testing procedures. The power gain of the amplifier is 18.7 dB at 300 MHz for each channel, which provides the sufficient RF transmission power for small animal parallel excitation applications at 7 T, particularly for high-channel-count transmission systems. Although the design was systematically tested using the standard RF testing procedures on bench, a test on phantoms and/or animals to acquire MR images with a dedicated multichannel RF transceive array is necessary to further evaluate the performance of the multi-channel transmit system developed in this work.

ACKNOWLEDGMENT

This work was supported in part by the National Natural Science Foundation of China Grant (51228702), and the National Institutes of Health (NIH) grant EB008699.

REFERENCES

1. Katscher U, Bornert P, Leussler C, van den Brink JS. 2003. "Transmit SENSE". Magn Reson Med 49:144–150.
2. Zhu Y. 2004. "Parallel excitation with an array of transmit coils". Magn Reson Med 51:775–784.
3. Grissom W, Yip CY, Zhang Z, Stenger VA, Fessler JA, Noll DC. 2006. "Spatial domain method for the design of RF pulses in multicoil parallel excitation". Magn Reson Med 56:620–629.
4. Zhang X, Pang Y. 2012. "Parallel excitation in ultrahigh field human MR imaging and multi-channel transmit system". OMICS J Radiol 1:e110.
5. Collins CM, Yang QX, Wang JH, Zhang X, Liu H, Michaeli S, et al. 2002. "Different excitation and reception distributions with a single-loop transmit-receive surface coil near a head-sized spherical phantom at 300 MHz". Magn Reson Med 47:1026–1028.
6. Yang QX, Wang J, Zhang X, Collins CM, Smith MB, Liu H, et al. 2002. "Analysis of wave behavior in lossy dielectric samples at high field". Magn Reson Med 47:982–989.
7. Zhang Z, Yip CY, Grissom W, Noll DC, Boada FE, Stenger VA. 2007. "Reduction of transmitter B1 inhomogeneity with transmit SENSE slice-select pulses". Magn Reson Med 57:842–847.
8. Liu Y, Feng K, McDougall MP, Wright SM, Ji J. 2008. "Reducing SAR in parallel excitation using variable-density spirals: a simulation-based study". Magn Reson Imaging 26:1122–1132.
9. Li Y, Wang C, Yu B, Vigneron D, Chen W, Zhang X. 2013. "Image homogenization using pre-emphasis method for high field MRI". Quant Imaging Med Surg 3:217–223.
10. Childs AS, Malik SJ, O'Regan DP, Hajnal JV. 2013. "Impact of number of channels on RF shimming at 3T". Magma 26:401–410.
11. Pang Y, Wu B, Jiang X, Vigneron DB, Zhang X. 2014. "Tilted microstrip phased arrays with improved electromagnetic decoupling for ultrahigh-field magnetic resonance imaging". Medicine (Baltimore) 93: e311.
12. Zhang X, Ugurbil K, Chen W. 2001. "Microstrip RF surface coil design for extremely high-field MRI and spectroscopy". Magn Reson Med 46:443–450.
13. Adriany G, Van de Moortele PF, Wiesinger F, Moeller S, Strupp JP, Andersen P, et al. 2005. "Transmit and receive transmission line arrays for 7 Tesla parallel imaging". Magn Reson Med 53:434–445.
14. Zhang X, Ugurbil K, Sainati R, Chen W. 2005. "An inverted-microstrip resonator for human head proton MR imaging at 7 tesla". IEEE Trans Biomed Eng 52: 495–504.
15. Wu B, Wang C, Kelley DA, Xu D, Vigneron DB, Nelson SJ, et al. 2010. "Shielded microstrip array for 7T human MR imaging". IEEE Trans Med Imaging 29:179–184.
16. Zhang X, Ugurbil K, Chen W. 2003. "A microstrip transmission line volume coil for human head MR imaging at 4T". J Magn Reson 161:242–251.
17. Yan X, Zhang X, Feng B, Ma C, Wei L, Xue R. 2014. "7T transmit/receive arrays using ICE decoupling for human head MR imaging". IEEE Trans Med Imaging 33:1781–1787.
18. Wu B, Zhang X, Wang C, Li Y, Pang Y, Lu J, et al. 2012. "Flexible transceiver array for ultrahigh field human MR imaging". Magn Reson Med 68:1332–1338.
19. Yan X, Zhang X, Wei L, Xue R. 2014. "Magnetic wall decoupling method for monopole coil array in ultrahigh field MRI: a feasibility test". Quant Imaging Med Surg 4:79–86.
20. Pang Y, Zhang X. 2011. "Precompensation for mutual coupling between array elements in parallel excitation". Quant Imaging Med Surg 1:4–10.
21. Li Y, Xie Z, Pang Y, Vigneron D, Zhang X. 2011. "ICE decoupling technique for RF coil array designs". Med Phys 38:4086–4093.
22. Zanchi MG, Stang P, Kerr A, Pauly JM, Scott GC. 2011. Frequency-offset Cartesian feedback for MRI power amplifier linearization. IEEE Trans Med Imaging 30:512–522.
23. Grissom WA, Kerr AB, Stang P, Scott GC, Pauly JM. 2010. Minimum envelope roughness pulse design for reduced amplifier distortion in parallel excitation. Magn Reson Med 64:1432–1439.
24. Hollingsworth N, Moody K, Nielsen JF, Noll DC, McDougall MP, Wright SM. 2011. An eight channel transmit system for Transmit SENSE at 3T. In: IEEE International Symposium on Biomedical Imaging: From Nano to Macro, March 30 2011–April 2 2011; Chicago, IL. p 775–778.
25. Gudino N, Heilman JA, Riffe MJ, Heid O, Vester M, Griswold MA. 2013. "On-coil multiple channel transmit system based on class-D amplification and pre-amplification with current amplitude feedback". Magn Reson Med 70:276–289.
26. Heilman JA, Riffe MJ, Heid O, Griswold MA. 2007. "High power, high efficiency on-coil current-mode amplifier for parallel transmission arrays". In: Proceedings of ISMRM. p 171, Berlin, Germany.
27. Hoult D, Kolansky G. 2008. "A 500 W, broadband, non-magnetic RF MOSFET amplifier for MRI use". In: Proceedings of ISMRM. p 1139, Toronto, Canada.
28. Lu J, Sun H. 2005. "Stability analysis of RF power amplifier". Foreign Electron Meas Technol 24:11–14.
29. Grebennikov A. 2005. RF and Microwave Power Amplifier Design. New York: McGraw-Hill.
30. Paul C. 2006. Introduction to Electromagnetic Compatibility. Hoboken: Wiley.